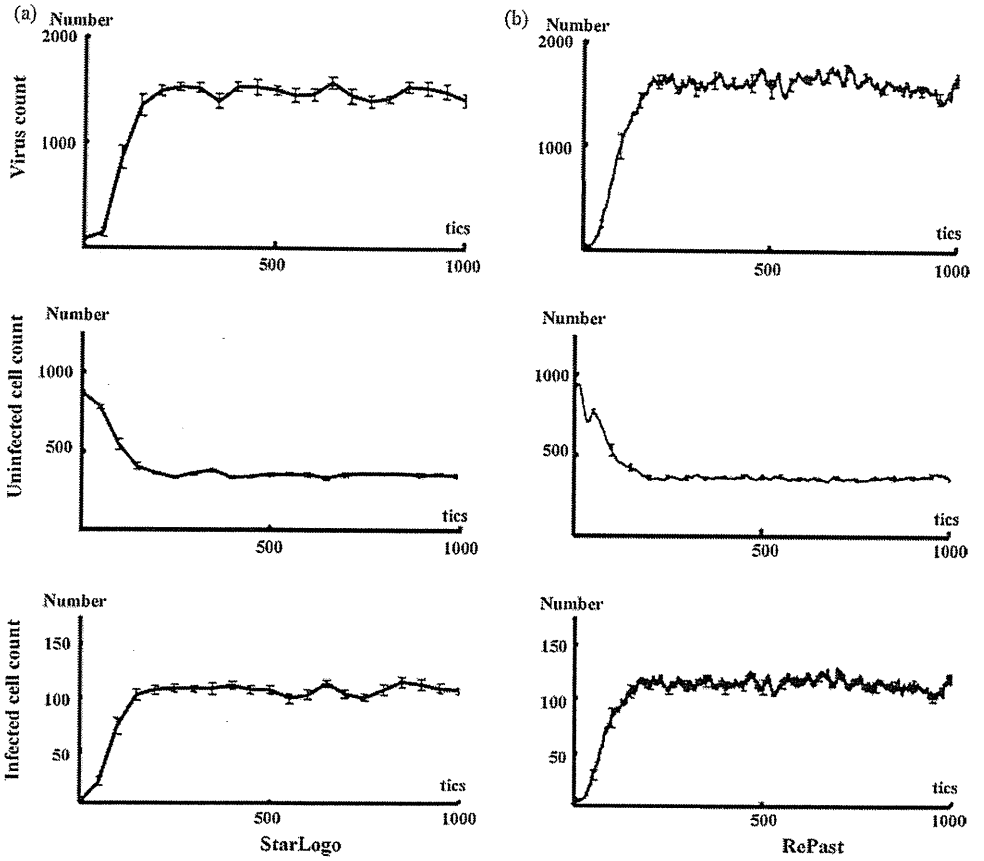

Fig. 2. Comparison of simulation results in (a) StarLogo and (b) RePast. The results were consistent when the parameters were made consistent. (Virus count [average ± SD]: StarLogo 1458.03 ± 173.1, RePast 1462.71 ± 178.8, $p = 0.94$. Uninfected cell count: 364.24 ± 30.4, 368.11 ± 33.4, $p = 0.83$. Infected cell count: 105.73 ± 13.0, 107.74 ± 13.0, $p = 0.24$. Unpaired Student's t-test.) Parameter values were set as follows: initial virus count, 100; uninfected cell count, 880; infected cell count, 0; virus speed of movement, 5 grids/tic; infection rate, 10%; uninfected cell regeneration rate, 1%; latent period, 3 tics; and virus reproduction rate, 5/cells/tic. The following parameter settings were taken from actual measurements: virus lifespan, 4.5 tics; uninfected cell lifespan, 49.8 tics; and infected cell lifespan, 6.7 tics.

immunodeficiency virus (HIV) (Ho et al., 1995), hepatitis B virus (HBV) (Nowak et al., 1996) and hepatitis C virus (HCV) (Neumann et al., 1998), and research is also underway on a range of models based on animal experiments and cell culture systems. As chronic viral disorders persist over long periods of time complete follow-up of viral dynamics is difficult. Furthermore, limitations of items that can be measured, such as the difficulty of measuring whole numbers of host cells, make it extremely difficult to investigate their consistency in mathematical models.

The recent ascend of dynamic-models owes much to advances in computers. Computer performance has improved markedly in recent years, not only in terms of their calculating capacity but also with regard to image displays, and models that offer a visual representation of viral disorders are now being reported (Gilbert and Bankes, 2002; Duca et al., 2007; Shapiro et al., 2008; Castiglione et al., 2007). One advantage of such visual models is that by providing a visual representation, they make understanding the disease status easy. Another benefit is that they enable parameters to be identified that are hidden as background noise in mathematical models. However, these models have some problems; it is difficult to prove the reproducibility of the simulation results derived from different languages or libraries, difficult to prove the validity of the model's concepts, and difficult to prove that the simulation results accurately reflect the reality. In this study, we created agent-based computer models that visually simulate the conditions of chronic viral infections using two software. The reproducibility of two agent-based computer models and the differences between agent-based models and the mathematical model were analyzed. This agent-based model enabled us to investigate how each parameter included in the concept affects the conditions of chronic viral infections.

2. Methods

2.1. Selection of Software

In this study, we used two different types of softwares: StarLogo version 2.0 (http://education.mit.edu/starlogo/) supplied by MIT Media Laboratory and Recursive Porous Agent Simulation Toolkit (RePast-3.0, http://repast.sourceforge.net/) supplied by the Argonne National Laboratory. StarLogo uses Logo, one of the simplest programming languages, and has a fixed graphical user interface. RePast is a library that uses Java, another programming language, which also has a fixed graphical user interface.

Logo is an assembly language, and StarLogo carries out processing sequentially. Java is an object-oriented language, and RePast has a faster processing speed than StarLogo. In addition, StarLogo has a number of stipulations to simplify simulations, such as parameters can only be set up to five decimal places and the simulation space is also fixed as 51 × 51 square grids. RePast, on the other hand, has fewer such restrictions. Thus, it offers a higher degree of freedom in program settings than StarLogo. Taking simulation space as an example, in spite of the restrictions imposed by the underlying operating system's image display system, any number of grids can be set and a hexagonal grid could also be chosen rather than a square one. However, users must stipulate and set all parameters themselves. This means that they must first declare the shape of the grid and the number of grids they will use to fill the simulation space. Java is also more difficult to learn than Logo, and debugging and correcting the program is also more difficult. Thus, it is difficult to judge whether or not the results agree with the planned simulation.

In effect, these two different types of softwares are polar opposites. It is simple to start a simulation in StarLogo, but producing results takes time and it is difficult to carry out more complex simulations. In RePast it is difficult to compose the program and judge whether or not the planned study has actually been achieved, but the

simulation itself takes only a short time to complete and there are lesser restrictions in the construction of a simulation model.

2.2. Concept for Modeling

We applied the basic virus–host interaction mathematical model to the agent-based simulation system with slight modifications. The mathematical model was used to describe the dynamics of HIV (Ho et al., 1995), HBV (Nowak et al., 1996), and HCV (Neumann et al., 1998) and the only agents involved were host cells and viruses, without the inclusion of immune cells. The effects of the immune system are expressed by varying parameters such as lifespan of host cells and viruses.

Fig. 1a illustrates the study concept. Viruses have the ability to infect healthy host cells (uninfected cells) and the infected cells produce new viruses. Both cells and viruses have definite lifespans, and the lifespan of infected cells is usually shorter than that of uninfected cells. Uninfected cells automatically regenerate within the space, whereas infected cells only arise due to infection of uninfected cells. Viruses also lack the ability to regenerate themselves and are only produced from infected cells.

2.3. Parameter Settings

In the present study, as the StarLogo settings are circumscribed, we limited the simulation space to 51 × 51 square grids. However, we made an exception here while investigating the effects of size of space on the simulation results. The numbers of viruses, uninfected cells, and infected cells could only be set before the start of the simulation. As described in the later, our simulation ran in cycles, with 1 cycle defined as 1 tic.

In mathematical simulation models, the death rate is required as a parameter. However, in our program we set lifespans for viruses and uninfected cells. These lifespans were not uniform, but were set to have a deviation of about 10%. The lifespan of cells was shortened by infection with ratio decided beforehand.

The infection ratio was meaningful only when an infected cell and a virus coincidentally occupied the same grid, and this was used to calculate the probability of the infection occurring in that situation. The virus production rate was set as the number of viruses produced by an infected cell during 1 tic. Infected cells could be set as a parameter indicating the latent period between the time of virus infection and the time of virus replication.

In order to emulate the tissue repair capacity, we set uninfected cell regeneration rate such that grids without any cells had a specified probability of producing uninfected cells on top of themselves. As a result, the more the cell count declined within a space the more regenerated uninfected cells were produced, whereas the number of regenerated cells declined as cell count increased.

The number of grids through which a virus could move in 1 tic was set as the speed of movement, and the direction of movement was set within a range of 90° toward the top of the simulation space. The program used a circulatory method of movement; when a virus arrived at the top of the space, it was translocated to the bottom, and moved again toward the top. Cells were fixed on the grid.

2.4. Simulation Flowchart

Fig. 1b shows a flowchart of the program. First, the simulation space was produced, after which each parameter was defined and the initial settings were made. Next the agents – viruses and uninfected and infected cells – were produced. The simulation cycle was as follows. Viruses moved to a new grid, and if an uninfected cell was present, this was infected with a probability based on the infection rate. The lifespan of the virus decreased, and viruses that had completed their lifespan and those that had caused an infection were removed from the space. Infected cells produced new viruses, the lifespans of both uninfected and infected cells decreased. Then, cells that had completed their lifespan were eliminated and a new cycle began. The program was set such that the simulation ended after this cycle had repeated 1000 times. This meant that one simulation was complete after 1000 tics.

2.5. Data Collection

The RePast model was programmed such that data for each tic was saved automatically as a text file at the end of the simulation. This text file could be opened by a database software. The StarLogo model was programmed to stop the simulation and collect data after every 50 tics.

2.6. Mathematical Model

In order to compare the results of this agent-based simulation, we used a viral infection mathematical model, which we improved as follows.

$$\frac{dT}{dt} = s[2601 - (T + I)] - dT - bVT \quad (1)$$

$$\frac{dI}{dt} = bVT - dI \quad (2)$$

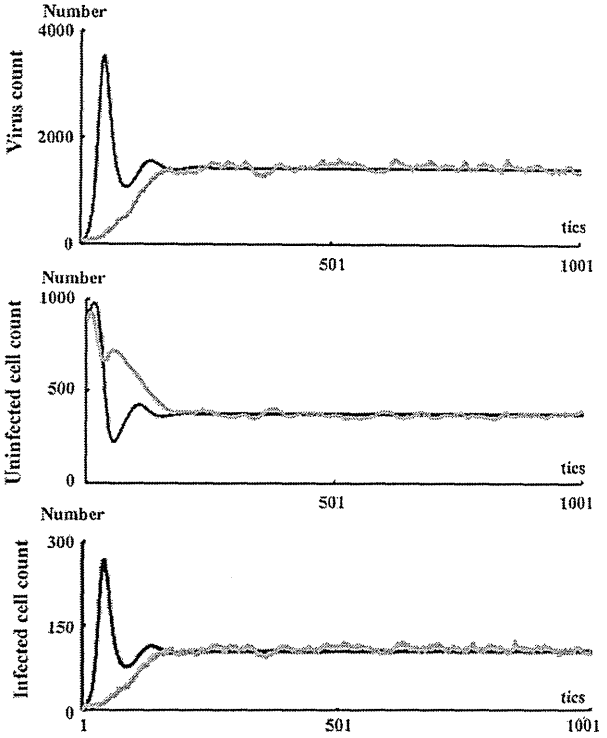

Fig. 3. Comparison of results of agent-based simulation and mathematical simulation. Both sets of results were consistent for the equilibrium phase, but differed in the shift in transition phase. Black line: mathematical model; grey line: results of simulation in RePast. Parameter values were set as follows: initial virus count, 100; uninfected cell count, 880; infected cell count, 0; virus speed of movement, 5 grids/tic; infection rate, 10%; uninfected cell regeneration rate, 1%; latent period, 3 tics; virus reproduction rate, 5/cells/tic; virus lifespan, 10 tics; uninfected cell lifespan, 50 tics; and cell lifespan-shortening ratio as a result of infection, 69%.

$$\frac{dV}{dt} = pI - cV \quad (3)$$

where, T is the uninfected cell count, I is the infected cell count, and V is the virus count. Uninfected cells are supplied to the space with a probability $s[2601 - (T+I)]$, as the number of grids in this agent-based simulation model was 2601 (51 × 51). The death rate of uninfected cells is d, the death rate of infected cells is δ, and the death rate of viruses is c. The infection rate is indicated by β. Viruses are released from infected cells at a probability p.

2.7. Statistical Analysis

Statistical analyses were performed by statistical tests using the program StatView 5.0 (SAS Institute Inc.). All tests of significance were two-tailed, with p values of <0.05 considered to be significant.

3. Results

3.1. Reproducibility of Chronic Viral Infection Disease Models Using Agent-based Simulation Methods

We constructed the chronic viral infection model with StarLogo library. Fig. 1c shows the simulation screen, and Fig. 1e shows one sample result. Immediately after the start of the simulation, the virus count temporarily dropped in accordance with the onset of an infection. Subsequently, the virus count started to increase with an increase in the infected cells and a decrease in the uninfected cells. After a certain number of tics (around 300 in this example), although the virus count, infected cell count, and uninfected cell count had some fluctuation, an equilibrium state was reached. We use the following descriptive terms in this paper: the transient phase is the period during which virus growth peaks, and the equilibrium phase is the period during which an equilibrium state is

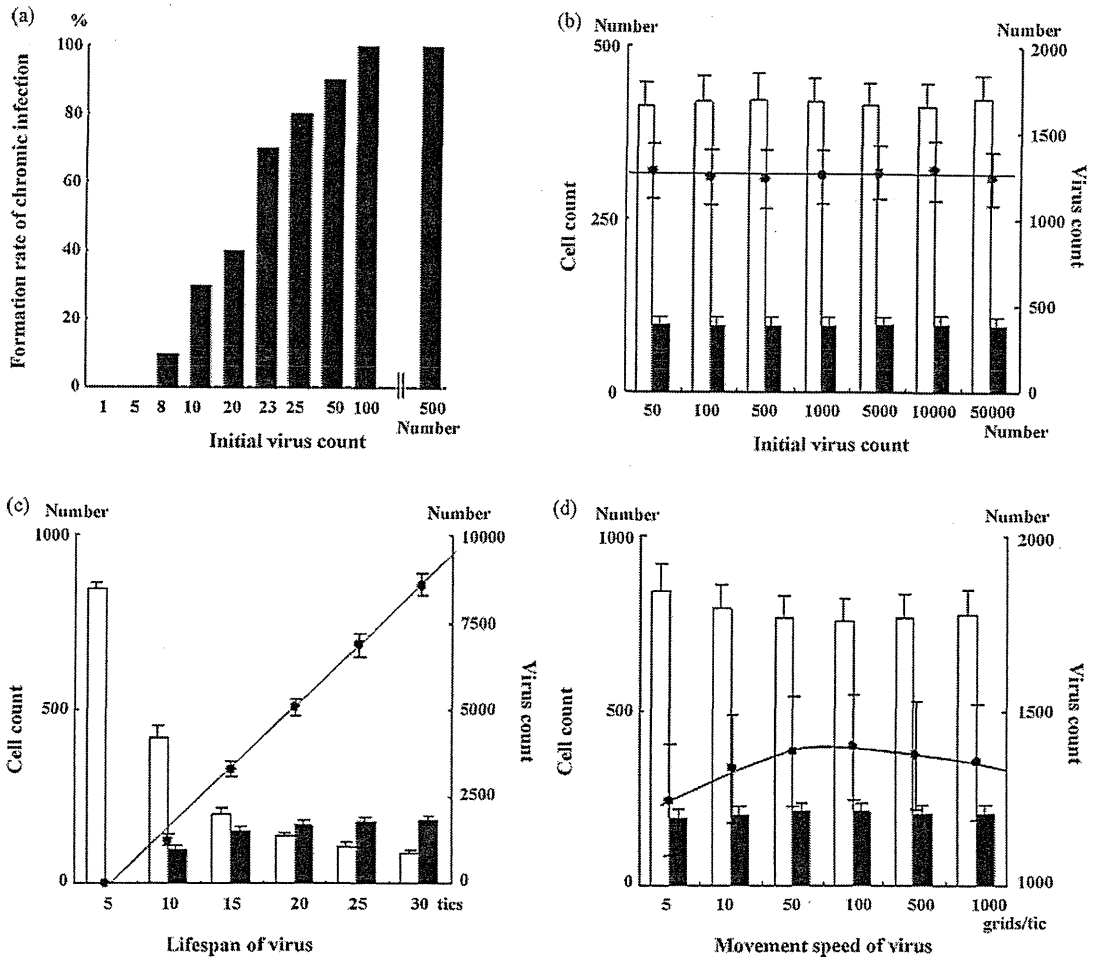

Fig. 4. *Effects of changes in viral parameters.* (a) The higher the initial virus count, the greater is the increase in the rate of formation of chronic infection, but (b) there was no effect on the conditions in the equilibrium phase. (c) Extending the virus lifespan increased the virus count. (d) Increasing the speed of virus movement to 100 grids/tic increased the virus count, but increasing it to 500 grids/tic had the opposite effect, with a slight declining trend. (a) Black bars: number of infections produced; (b–d) black circles: virus count; line: virus count approximation curve; white bars: uninfected cell count; black bars: infected cell count.

established. When the simulation was performed multiple times, the features described above were maintained, and the average values for virus, infected cell, and uninfected cell counts during the equilibrium state were all consistent.

Fig. 1d shows the simulation screen of the RePast. When we attempted setting all the initial parameters to the same values as those in the StarLogo, the results were not consistent. When we recalculated the parameters from the simulation results, in RePast, the parameters were largely maintained at the levels of the settings, but in StarLogo, the lifespans of both cell types became shorter than the settings while the simulation was in progress. We made the results of both simulations consistent by using the same parameters during the actual simulation (Fig. 2a and b).

3.2. Comparison Between Agent-based Simulation Models and Mathematical Simulation Model

We investigated whether the results of a chronic viral infection disease model produced by RePast would be consistent with the results of a mathematical model. For the mathematical model, we carried out an approximate integration using a four-dimensional Runge–Kutta method to ensure that the uninfected cell count and infected cell count would be in the same class. Parameters were always fixed as constant between simulations. The simulation results were consistent for the equilibrium phase, but transitions in virus count during the transient phase varied, with a shift to equilibrium state following two overshoots in the mathematical model, but a monotonic increase following a logistic curve in the agent-based model (Fig. 3). In the mathematical model, when the equilibrium condition was calculated with $dT/dt = dI/dt = dV/dt = 0$, the equilibrium-phase virus count, uninfected cell count, and infected cell count were very similar to those of the agent-based model (virus count: mathematical model 371.8/space, agent-based model 371.1 ± 32.4/space [average ± SD]; uninfected cell count: mathematical model 1605/space, agent-based model 1454 ± 194/space; infected cell count: mathematical model 115.9/space, agent-based model 108.3 ± 14.2/space).

3.3. Usability of the Models; Effect of Changing Parameters

We investigated the changes in the equilibrium phase brought about by changing each parameter. All the investigations below were carried out by using RePast, and we used the average values from ten simulations.

3.4. Viral Parameters

The lower the virus counts at the beginning of the simulation, the lower the probability of a chronic infection (Fig. 4a). However, the initial virus count did not have any effect on the equilibrium

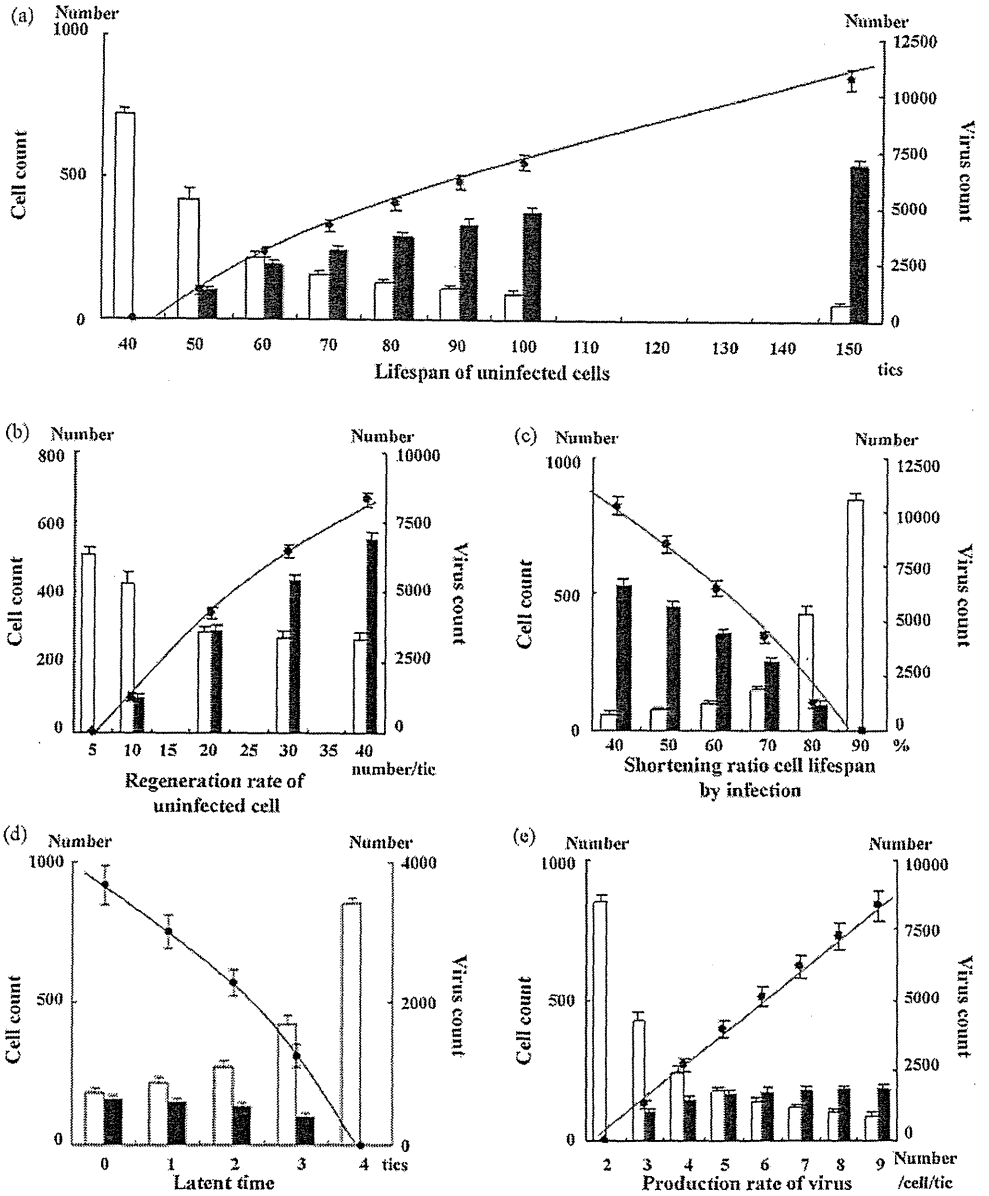

Fig. 5. Effects of changes in cell parameters. (a) Extending the uninfected cell lifespan and (b) increasing the uninfected cell regeneration rate increased the virus count. (c) Raising the lifespan-shortening ratio as a result of infection shortened the lifespan of infected cells, thereby decreasing the virus count. (d) Extending the latent period shortened the period of virus production from infected cells, thereby decreasing the virus count. (e) Increasing the virus production count resulted in a linear increase in equilibrium-phase virus count. Black circles: virus count; line: virus count approximation curve; white bars: uninfected cell count; black bars: infected cell count.

phase itself (Fig. 4b). Extending the lifespan of viruses resulted in a linear increase in equilibrium-phase virus count (Fig. 4c). Although the infected cell count increased, the rate of increase gradually declined. Changing the speed of viral movement resulted in the equilibrium-phase virus count to eventually decline after 100 grids/tic was reached, allowing movement over an area twice the size of the simulation space (Fig. 4d).

3.5. Uninfected Cell Parameters

Extending the lifespan of uninfected cells led to an increased virus count during the equilibrium phase (Fig. 5a). Increasing the uninfected cell regeneration rate also contributed to increased equilibrium-phase virus count (Fig. 5b). In both the cases, the increases in virus count and infected cell count were not linear, but showed a tendency for the rate of increase to decline gradually.

3.6. Infected Cell Parameters

We carried out an investigation of the effects of variation in the lifespan-shortening ratio on the virus count on the assumption that cell lifespan is shortened by infection. When this ratio was increased, the virus count decreased (Fig. 5c). An extended latent period was also related to a decreased virus count (Fig. 5d). However, the virus production from infected cells led to a linear increase in the virus count (Fig. 5e).

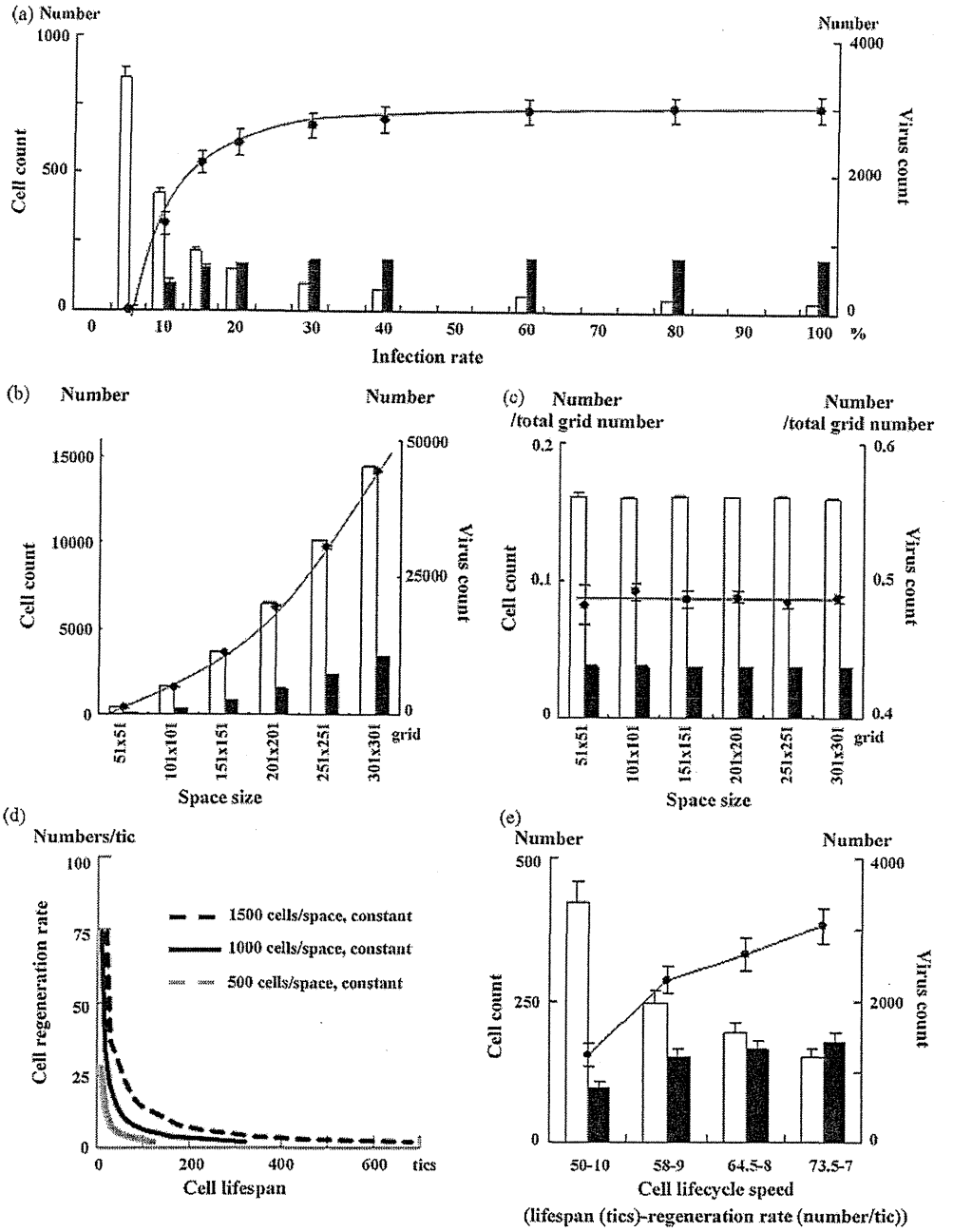

Fig. 6. (a) Increasing the infection rate increased the virus count in equilibrium periods, but the virus count did not change at infection rates of 30% or more. (b) The size of the simulation space increased not only virus count but also the cell count; however, (c) when virus and cell counts were divided by the total number of grids in the space, they were constant for all space sizes. (d) Changing the lifespan and regeneration rate of uninfected cells in opposite directions at the same time makes it possible to change only the cell cycle speed without altering the uninfected cell count. (e) When the cell cycle speed was reduced, the virus count increased toward the right of the graph. This may be because the effect of extending the lifespan of cells exceeds that of reducing their regeneration rate. (a–c and e) Black circles: virus count; line: virus count approximation curve; white bars: uninfected cell count; black bars: infected cell count.

3.7. Infection Rate and Space Size

Increasing the infection rate caused an increase in the virus count, but the change was minimal at an infection rate of 30% or more. The same results were seen for infected cell count, but a decrease in uninfected cell count resulted in a tendency for the infection rate to decrease by up to 60% (Fig. 6a).

The larger the space, higher the increase in both virus and cell counts (Fig. 6b). This increase was proportional to space size, however, when virus and cell counts were divided by the total number of grids in the space they were all constant (Fig. 6c).

3.8. Cell Cycle Speeds

Running a simulation with the initial virus count set to zero enables only the equilibrium condition for uninfected cells to be simulated. Changing the lifespan and regeneration rate of uninfected cells in opposite directions at the same time makes it possible

to change the cell cycle speed without altering the uninfected cell count (Fig. 6d). We used this technique to investigate how changing the cell cycle speed affected the equilibrium phase. Fig. 6e shows the results. Cell lifespan increases while the cell cycle speed declines. The equilibrium virus count increased in accordance with slower cell cycle speeds.

4. Discussion

In this study, we investigated the models using two agent-based simulation methods to program a simple virus–host chronic infection model. The same model written in two different programming language systems displayed the same results. The transient phase was unlike that seen in a mathematical simulation with no overshoot in virus count, but rather a smooth transition to the equilibrium phase. The virus count at the start of the simulation only had effect on the rate of infection development. Increases in virus lifespan, uninfected cell lifespan, uninfected cell regeneration rate, virus production count from infected cells, and infection rate all led to increased equilibrium-phase virus count. Rises in the infected cell lifespan-shortening ratio, latent period, and cell cycle speed decreased the equilibrium-phase virus count. The size of the space itself had no innate effect on the equilibrium phase, but a speed of movement of the virus that was twice the size of the space produced the maximum virus count.

Reproducibility is the basis for all scientific study, but there are many problems to prove it in computer simulations, such as programming bugs. As agent-based simulation deals with numerous agents individually, it requires vast amounts of calculations. Accumulation of very small change of values leads to large differences of results. In this study, we investigated two programs based on two programming languages to confirm the reproducibility of our simulation results in different programming languages. The results of two simulations were consistent, but in StarLogo, the lifespan parameters had a tendency to be lower than when they were set while simulations were actually in progress. This may be because the number of digits used in calculations was different between the two programs. RePast performs calculations to at least eight decimal places. In StarLogo, the library settings only enable settings to be made up to five decimal places. It is probable that these small differences accumulate during repeated calculations and are reflected in the simulation. Ultimately, we confirmed that the differences in results obtained by using different libraries and programming languages were not innate and by making the parameters consistent during simulation, consistent results were obtained.

Mathematical models using formulae for HIV therapy was published in 1994, the method has since been applied to HBV and HCV (Ho et al., 1995; Nowak et al., 1996; Neumann et al., 1998), and they were thought to be good reflections of the reality. In the mathematical model, viruses and cells are conceived as individuals in the concept itself, but both of them are perceived *en masse* when calculations are performed. However a feature of the agent-based simulation is that it deals with individual viruses and cells as separate agents. By moving each agent individually, it probes the factors influencing overall shifts from the micro viewpoint. When the space is viewed as a whole, it is possible to watch on the screen the collective movement of groups of agents. Recently, models that provide a visual representation of Epstein-Barr virus and HIV infection have been reported, both of which are useful for an instinctive and intuitive understanding (Duca et al., 2007; Shapiro et al., 2008; Castiglione et al., 2007).

In agent-based simulation model, virus count transit smoothly to the equilibrium phase. On the other hand, virus counts overshoot during transient phase in mathematical model. We think this difference is derived from technicality of different modeling. The difference in concepts between mathematical models and agent-based models is the space. The mathematical model has no space in concept, but agents move across the space in the agent-based model. In agent-based models, the densities of virus and cells change overtime especially in the transition phase because of the limited space. These changes of the densities of virus and cells lead to the dynamic change of the encounter rate of viruses and cells. The mathematical model does not make such concept of the density; the encounter rate is constant. This may be the reason for the difference between two models in the transition phase. Since no overshoot of virus counts in transient phase had been reported from in vivo studies of hepatitis C virus and simian immunodeficiency virus (Dahari et al., 2005; Nowak et al., 1997), agent-based model correlates with actual biology in vivo at least for these viruses. The increase of initial virus count at the start of simulation correlates with higher encounter rate of viruses and cells which make the linear increasing of infection forming rate. Mathematical model can only express the infection formation rate as "infected or not".

The importance of viral passing speed in the agent-based model is also explained by the "space". Although the virus actually moves through the blood stream in our body and virus could not decide their moving speeds by themselves, there is most appropriate speed for virus to meet the cells on the simulation space by the highest probability. The effect of cell cycle speed should be mentioned by another affection of the space. A fast cell cycle speed means that the lifespan of uninfected cells is short. Then fast cell cycle speed leads to the short lifespan of infected cells. A higher regeneration rate for uninfected cells results in a higher rate of infection among uninfected cells by viruses, but in situations where viruses and cells are dispersed around the space this is ineffective in increasing the infection rate, as the latter depends on the probability that they will encounter one another. As a result, the infected cell count decreases during the equilibrium phase, as does the virus count.

In this study, we confirmed the reproducibility and usability of agent-based models in expressing the interaction between viruses and cells. A feature of this simulation system is that it uses the concept of space as actual space, which means that the existence of the space becomes an additional controlling factor on the simulation results. This is a concept that is absent from mathematical models. The reality is that we have a spatial existence, and an advantage of the agent-based simulation system is the fact that it accounts for the space. Another feature of the simulation system is that it enables the condition to be perceived in visual terms, making it easy to understand. However it may be affected by computer performance and by the limitations of programming languages or the program itself, this system may offer a powerful tool for the future analysis of real virus–host interaction disease.

Conflict of interest

No conflicts of interest exist for all authors.

References

Castiglione, F., Pappalardo, F., Bernaschi, M., Motta, S., 2007. Optimization of HAART with genetic algorithms and agent-based models of HIV infection. Bioinformatics 23, 3350–3355, doi:10.1093/bioinformatics/btm408.

Dahari, H., Major, M., Zhang, X., Mihalik, K., Rice, C.M., Perelson, A.S., Feinstone, S.M., Neumann, A.U., 2005. Mathematical modeling of primary hepatitis c infection: noncytolytic clearance and early blockage of virion production. Gastroenterology 128, 1056–1066, doi:10.1053/j.gastro.2005.01.049.

Duca, K.A., Shapiro, M., Delgado-Eckert, E., Hadinoto, V., Jarrah, A.S., Laubenbacher, R., Lee, K., Luzuriaga, K., Polys, N.F., Thorley-Lawson, D.A., 2007. A virtual look at Epstein-Barr virus infection: biological interpretations. PLoS Pathog. 3, 1388–1400, doi:10.1371/journal.ppat.0030137.

Gilbert, N., Bankes, S., 2002. Platforms and methods for agent-based modelling. Proc. Natl. Acad. Sci. U.S.A. 99 (Suppl. 3), 7197–7198.

Ho, D.D., Neumann, A.U., Perelson, A.S., Chen, W., Leonard, J.M., Markowitz, M., 1995. Rapid turnover of plasma virions and CD4 lymphocytes in HIV-1 infection. Nature 373, 123–126, doi:10.1038/373123a0.

Naniche, D., 2009. Human immunology of measles virus infection. Curr. Top. Microbiol. Immunol. 330, 151–171.

Neumann, A.U., Lam, N.P., Dahari, H., Gretch, D.R., Wiley, T.E., Layden, T.J., Perelson, A.S., 1998. Hepatitis C viral dynamics in vivo and the antiviral efficacy of interferon-alpha therapy. Science 282, 103–107, doi:10.1126/science.282.5386.103.

Nowak, M.A., Bonhoeffer, S., Hill, A.M., Boehme, R., Thomas, H.C., McDade, H., 1996. Viral dynamics in hepatitis B virus infection. Proc. Natl. Acad. Sci. U.S.A. 93, 4398–4402.

Nowak, M.A., Lloyd, A.L., Vasquez, G.M., Wiltrout, T.A., Wahl, L.M., Biscofberger, N., Williams, J., Kinter, A., Fauci, A.S., Hirsch, V.M., Lifson, J.D., 1997. Viral dynamics of primary viremia and antiretroviral therapy in simian immunodeficiency virus infection. J. Virol. 71, 7518–7525.

Shapiro, M., Duca, K.A., Lee, K., Delgado-Eckert, E., Hawkins, J., Jarrah, A.S., Laubenbacher, R., Polys, N.F., Hadinoto, V., Thorley-Lawson, D.A., 2008. A virtual look at Epstein-Barr virus infection: simulation mechanism. J. Theor. Biol. 252, 633–648, doi:10.1016/j.jtbi.2008.01.032.

See, H., Wark, P., 2008. Innate immune response to viral infection of the lungs. Paediatr. Respir. Rev. 9, 243–250, doi:10.1016/j.prrv.2008.04.001.

Comparison of Hepatitis B Virus DNA, RNA, and Core Related Antigen as Predictors of Lamivudine Resistance in Patients with Chronic Hepatitis B

Akihiro MATSUMOTO, Noboru MAKI, Kaname YOSHIZAWA
Takeji UMEMURA, Satoru JOSHITA, and Eiji TANAKA

信 州 医 学 雑 誌
別 刷
第 58 巻 第 4 号

Comparison of Hepatitis B Virus DNA, RNA, and Core Related Antigen as Predictors of Lamivudine Resistance in Patients with Chronic Hepatitis B

Akihiro MATSUMOTO[1)], Noboru MAKI[2)], Kaname YOSHIZAWA[1)]
Takeji UMEMURA[1)], Satoru JOSHITA[1)] and Eiji TANAKA[1)]*

1) *Department of Medicine, Gastroenterology, Shinshu University School of Medicine*
2) *R&D Division, Advanced Life Science Institute, Inc.*

The clinical usefulness of hepatitis B virus (HBV) DNA, RNA, and core related antigen (HBcrAg) assays for predicting the appearance of HBV DNA breakthrough was evaluated and compared in patients with chronic hepatitis B undergoing lamivudine therapy. Methods : Thirty six patients with chronic hepatitis B who received lamivudine therapy for more than 1 year were enrolled. HBV RNA was measured simultaneously with HBV DNA (HBV RNA/DNA) using a real-time detection polymerase chain reaction assay with a preceding step of reverse-transcription. HBV DNA was measured by an HBV AMPLICOR monitor kit. HBcrAg was measured using a chemiluminescence enzyme immunoassay. Results : Sixteen patients (44 %) developed HBV DNA breakthrough during the median observation period of 48.4 months (range 7.4-87.8 months). Afterwards, HBV DNA breakthrough was prospected using the three parameters taken 6 months after starting lamivudine therapy. The cut-off levels for predictions were determined by receiver operating characteristic curves, and were 2.6 log copies/ml for HBV DNA, 3.8 log U/ml for HBV RNA/DNA, and 4.0 log U/ml for HBcrAg. Sensitivity, specificity, and accuracy for predicting HBV DNA breakthrough were 25 %, 100 %, and 67 % respectively for HBV DNA. Similarly, they were 50 %, 90 %, and 72 % for HBV RNA/DNA, and 100 %, 40 %, and 67 % for HBcrAg. Conclusion : Our findings confirm that HBV DNA is useful for identifying patients who are at high risk for HBV breakthrough. HBcrAg is useful for isolating those who are at low risk, and HBV RNA/DNA showed predictive characteristics similar to HBV DNA with higher sensitivity and the highest accuracy. *Shinshu Med J 58 : 153—162, 2010*

(Received for publication March 17, 2010 ; accepted in revised form May 7, 2010)

Key words : hepatitis B virus, HBV core related antigen, HBV RNA, lamivudine, breakthrough

I Introduction

Lamivudine (LAM), a nucleoside analogue, inhibits the replication of hepatitis B virus (HBV), reduces hepatitis, and improves histological findings of the liver during long-term therapy. Lamivudine treatment has also been reported to reduce the risk of complicating hepatocellular carcinoma[1)2)]. However, relapse of hepatitis due to the appearance of resistant viruses is a major drawback of lamivudine therapy[3)-5)]. Recently, new nucleoside and nucleotide analogues have been developed, such as adefovir dipiboxil and entecavir, which develop resistant viruses far less frequently than

* Corresponding author : Eiji Tanaka
Department of Medicine, Shinshu University School of Medicine, 3-1-1, Asahi, Matsumoto-city, Nagano-prefecture, 390-8621, Japan

Abbreviations : HBV, hepatitis B virus ; HBcrAg, hepatitis B virus core related antigen ; HBV RNA/DNA, hepatitis B virus RNA and DNA ; LAM, lamivudine ; YMDD, tyrosine-methionine-aspartic acid-aspartic acid ; HBsAg, hepatitis B virus surface antigen ; HBeAg, hepatitis B virus e antigen ; HBeAb, anti-hepatitis B antibody ; RTD-PCR, real-time detection polymerase chain reaction assays ; ROC, receiver operating characteristic ; cccDNA, covalently closed circular DNA.

lamivudine, but these analogues still face the problem of resistant viruses[6)-8)].

The concentration of HBV DNA in serum decreases and usually becomes undetectable during lamivudine administration[9)-12)], but can rapidly increase when tyrosine-methionine-aspartic acid-aspartic acid (YMDD) mutations induce lamivudine resistant strains[13)-16)]. Thus, the measurement of HBV DNA is useful for monitoring the anti-viral effects of lamivudine, but monitoring these effects by HBV DNA level alone is not satisfactory because lamivudine resistance occurs even in patients who show undetectable levels of serum HBV DNA[13)17)18)].

We previously described a HBV core-related antigen (HBcrAg) assay[19)] which measures the total amount of protein encoded by the pre-core and core regions of the HBV genome, including core, e, and p22cr[20)] antigens. In those experiments, the serum level of HBcrAg was shown to be useful for predicting the occurrence of lamivudine resistance in a manner different from serum levels of HBV DNA[21)]. We also reported that serum HBV RNA is detectable in a form incorporated into virus particles in patients with hepatitis B undergoing lamivudine therapy, which could possibly represent a new viral marker of different significance than that of HBV DNA in lamivudine therapy[22)].

Thus, in the present study, we sought to compare the clinical usefulness of using HBV DNA, HBV RNA, and HBcrAg to predict the occurrence of lamivudine resistance, as detected by HBV DNA breakthrough in patients with chronic hepatitis B receiving lamivudine therapy.

II Patients and Methods

A Patients

A total of 36 patients with chronic hepatitis B who started LAM therapy at Shinshu University Hospital between July 2002 and February 2004 were enrolled in this study. They consisted of 28 men and 8 women and had a median age of 55 years (range 29-80 years) at the commencement of LAM therapy. Chronic hepatitis B was defined as positive for HBV surface antigen (HBsAg) for more than 6 months with liver histological findings consistent with chronic hepatitis. All patients had elevations in serum alanine aminotransferase (ALT) levels, as well as detectable HBV DNA for at least 6 months. Immediately prior to LAM administration, 23 of the patients were positive for HBV e antigen (HBeAg) and 13 were positive for anti-HBV e antibody (HBeAb) and negative for HBeAg. The HBV genotype was C in all patients except three (two were genotype B and one was F). Patients received 100 mg doses of LAM daily for at least 12 months. No patient underwent treatment with any other anti-viral agent, such as interferon, before or during the present study, and all patients were negative for hepatitis C and human immunodeficiency virus antibodies. Written informed consent was obtained from each patient. This study was approved by the Ethics Committee of Shinshu University.

Serum samples were collected from the start of LAM therapy on a monthly basis and were stored frozen at −20 °C or below until assayed. The occurrence of LAM resistance was defined as a rapid increase in serum HBV DNA with the appearance of the YMDD mutations. Using these criteria, resistance appeared in 16 (44 %) of the 36 patients. The median period from the start of LAM therapy to the occurrence of resistance was 18.2 months, with a range of 7.4 to 57.7 months.

B Routine laboratory tests

Serological markers for HBV, including HBsAg, HBeAg, and HBeAb, were tested using commercially available enzyme immunoassay kits (Abbott Japan Co., Ltd., Tokyo, Japan). Six HBV genotypes (A-F) were evaluated according to the restriction patterns of DNA fragments from the method reported by Mizokami et al[23)]. The YMDD motif, a LAM-resistant mutation in the active site of HBV polymerase, was detected using an enzyme-linked mini-sequence assay kit (HBV YMDD Mutation Detection Kit, Genome Science Laboratories Co., Ltd., Tokyo, Japan)[24)]. Serum concentration of HBV DNA was determined using an AMPLICOR HBV monitor kit (Roche, Tokyo, Japan), which had a

quantitative range of 2.6 to 7.6 log copies/ml.

C HBV core-related antigen assay

Serum HBcrAg was measured using a chemiluminescence enzyme immunoassay (CLEIA) as reported previously[25]. In brief, 100 μl aliquots of serum were mixed with pretreatment solution containing 15 % sodium dodecylsulfate. After incubation at 70 °C for 30 min, 50 μl pretreated serum was added to wells coated with monoclonal antibodies against denatured HBV core and e antigens (HB44, HB61, and HB114) and filled with 100 μl assay buffer. The mixture was then incubated for 2 hrs at room temperature. After washing with buffer, either alkaline phosphatase-labeled HB50 monoclonal antibody (specific for denatured HBV core antigen) or a mixture of HB91 and HB110 monoclonal antibodies (specific for denatured HBV core and e antigens) were added to wells and incubated for 1 hr at room temperature. After washing again, CDP-Star with Emerald II (Applied Biosystems, Bedford, MA) was added and plates were incubated for 20 min more at room temperature. The relative chemiluminescence intensity was measured, and HBcrAg concentrations were read by comparison to a standard curve generated with recombinant pro-hepatitis B e antigen (amino acids -10 to 183 of the precore/core gene product). The concentration of HBcrAg was expressed as units/ml and the immunereactivity of recombinant pro-hepatitis B e antigen at 10 fg/ml was defined as 1 unit/ml. The lower detection limit of this assay was set at 2 log units/ml. Sera containing over 7 log units/ml of antigen were diluted 10 or 100 fold in normal human serum and measured again to obtain the end titer.

D HBV RNA/DNA

The High Pure Viral Nucleic Acid Kit (Roche Diagnostics) was used for isolation of HBV DNA and RNA from serum. Briefly, 200 μl of serum was added to 250 μL of freshly prepared working solu tion (6 M guanidine-HCl, 10 mM urea, 10 mM Tris-HCl [pH 4.4] and 20 % [vol/vol] Triton X-100) supplemented with 20 μg of poly (A) carrier RNA and 900 μg of Proteinase K. After incubation for 10 min at 72 °C, 100 μl of isopropanol was added and the mixture was transferred into a High Pure filter tube fitted with a collection tube. The filter tube was centrifuged for 1 min at 8,000 rpm in a standard tabletop centrifuge at room temperature, then attached to a new collection tube. An inhibitor removal buffer (5 M guanidine-HCl, 20 mM Tris-HCl [pH 6.6] in ethanol) was added to the upper reservoir and the tube was centrifuged again for 1 min at 8,000 rpm. After being washed with 250 μl of wash buffer (20 mM NaCl, 2 mM Tris-HCl [pH 7.5] in ethanol), the filter was placed in a new collection tube and 50 μl of RNase-and DNase-free water was added to elute the DNA and RNA. After centrifugation for 1 min at 8,000 rpm, the eluted DNA and RNA was stored at −80 °C. Synthesis of cDNA was performed at 42 °C for 30 min in a 20 μl reaction mixture containing 10 μL of the extracted DNA and RNA, 50 mM Tris-HCl (pH 8.3), 75 mM KCl, 3 mM $MgCl_2$, 1 mM dNTP (1 mM each dATP, dGTP, dCTP and dTTP), 1 mM DTT, 100 nM reverse primer for the HBV surface gene (5'-GGTTGGTGAGTGATTGGAGGTT-3' ; nt. 345 to 324), 40 units of RNasin (TaKaRa, Kyoto, Japan), and 200 units of SuperScript II RNase H- Reverse Transcriptase (Invitrogen, Carlsbad, CA). The reaction mixture was inactivated by heating to 70 °C for 15 min, then cooled to -80 °C until real-time detection polymerase chain reaction (RTD-PCR) assays. A 4 μl aliquot of DNA and cDNA solution was used for RTD-PCR, which was performed with the Light Cycler System (Roche Diagnostics) as reported previously[25]. The two primers and TaqMan probe used were designed from a region of the HBV surface gene : forward primer ; 5'-ACAACATCAG-GATTCCTAGGAC-3' (nt. 166 to 187), reverse primer as stated above (nt. 345 to 324), and TaqMan probe ; 5'-FAM-CAGAGTCTAGACTCGTGGTG-GACTTC-TAMRA-3' (nt. 244 to 269). An HBV genome (nt. 20 to 1805) subcloned into a pUC vector was used as an internal standard. The lower detection limit for the HBV RNA/DNA assay was set at 2.6 log copy/ml.

E Statistical analysis

The proportion of each clinical factor was

compared between the groups with or without HBV DNA breakthrough using the χ^2 and Fisher's exact probability tests, and group medians were compared using the Mann-Whitney's U test. Correlations between HBV RNA/DNA and HBV DNA or HBcrAg were tested using Spearman's analysis. The rates of HBV DNA breakthrough during LAM treatment between higher and lower level groups of HBV DNA, HBcrAg and HBV direct RT-PCR were analyzed using the Kaplan-Meier method, and the difference in incidences was assessed with the log-rank test. Receiver operating characteristic (ROC) curves were used to decide each cut-off point for predicting HBV DNA breakthrough. All tests were performed using the SPSS 10.0 J statistical software package (SPSS Inc., Chicago, IL). P values less than 0.05 were considered significant.

III Results

A Comparison of characteristics between patients with and without HBV DNA breakthrough

HBV DNA breakthrough occurred in 16 (44.4 %) of 36 patients during the follow-up period. The cumulative HBV DNA breakthrough incidence in all patients was 8.3 % at 12 months, 27.8 % at 24 months, 33.5 % at 36 months, 40.2 % at 48 months, and 48.2 % at 60 months. The clinical characteristics at baseline in the 16 patients with HBV DNA breakthrough and 20 patients without are shown in Table 1. The median follow-up period did not differ, and no significant differences were observed in any other characteristics, including ALT, HBV DNA, HBcrAg, and HBV RNA/DNA.

B Changes in serum HBV DNA, HBcrAg and HBV RNA/DNA

Changes in serum levels of HBV DNA, HBcrAg, and HBV RNA/DNA from baseline to 6 months of lamivudine therapy are shown in Fig. 1. HBV DNA decreased rapidly and became undetectable within 6 months in all except 4 patients with HBV DNA breakthrough. HBcrAg decreased more slowly than HBV DNA, and became undetectable only in 2 (6 %) of the 36 patients at 6 months. HBV RNA/DNA decreased faster than HBcrAg, but slower than HBV DNA, and became undetectable at 6 months in 15 (42 %) of the 36 patients.

Although HBV RNA/DNA was significantly correlated with both HBV DNA (Fig. 2A) and HBcrAg (Fig. 2B) at the start of lamivudine therapy, this association was lost at 6 months because over 90 % of patients became undetectable for HBV DNA (Fig. 2C). On the other hand, HBV RNA/DNA retained its correlation with HBcrAg at 6 months (Fig. 2D). Although significant, the HBcrAg to HBV RNA/DNA ratio tended to be lower when compared to baseline.

C Prediction of occurrence of lamivudine resistance

The occurrence of lamivudine resistance was next prospected using the levels of HBV DNA, HBcrAg, and HBV RNA/DNA measured at 6

Table 1 Baseline characteristics of patients with and without HBV DNA breakthrough during lamivudine therapy

	with breakthrough	without breakthrough	p
Number	16	20	
Age (y.o.)[a]	56.0 (29.5−64.0)	53.6 (41.0−79.5)	0.660
Gender (male/female)	13/3	15/5	1.000
Follow-up period (months)[a]	53.2 (21.5−84.0)	67.5 (45.8−89.5)	0.421
HBeAg (+/−)	10/6	9/11	0.508
HBeAb (+/−)	6/10	11/9	0.508
ALT (IU/l)[a]	60 (22−499)	119 (20−1816)	0.156
HBV DNA (log copy/ml)[a]	6.7 (4.8−>7.6)	6.1 (3.9−>7.6)	0.338
HBcrAg (log U/ml)[a]	5.9 (4.3−8.2)	5.8 (2.9−8.7)	0.683
HBV RNA/DNA (log U/ml)[a]	6.2 (4.8−8.3)	6.3 (4.4−8.8)	0.916

[a] Data are expressed as median (range)

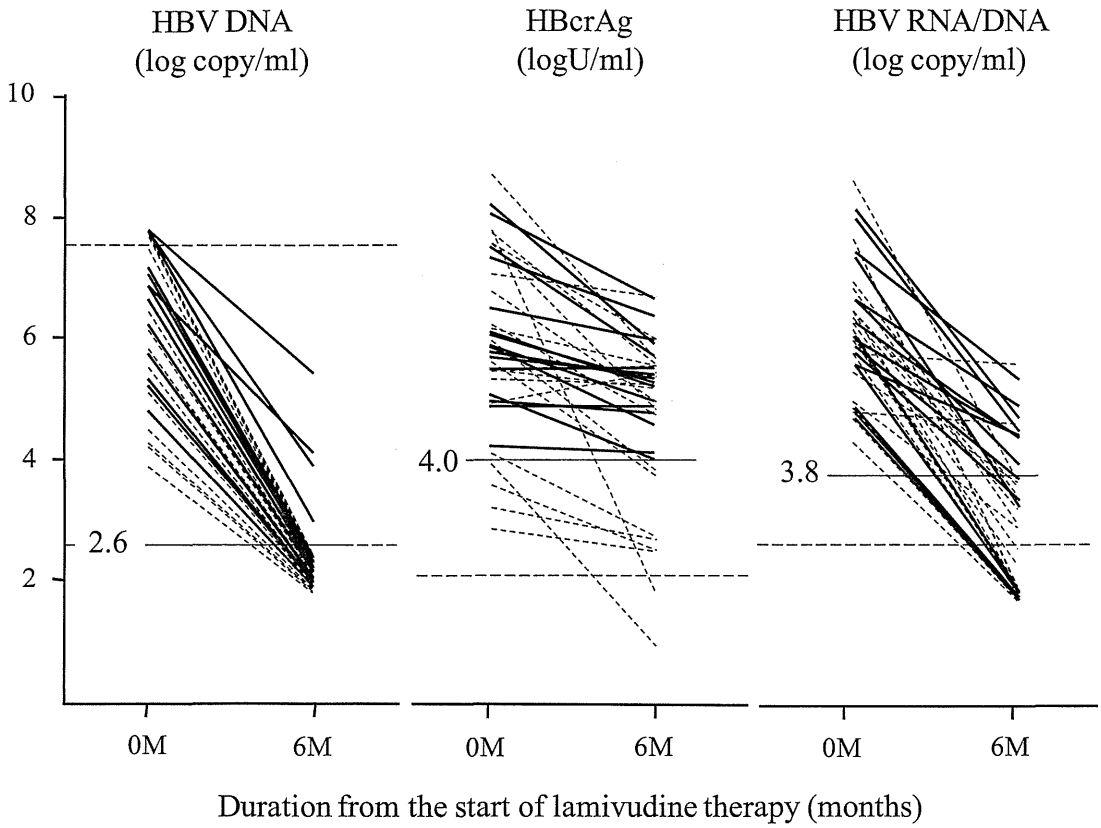

Fig. 1 Changes in serum levels of HBV DNA, HBcrAg, and HBV RNA/DNA from baseline to month 6. The solid line indicates patients with HBV DNA breakthrough during the observation period, and the broken line indicates patients without. The horizontal broken line indicates the lower detection limit of each assay. Cut-off values for predicting lamivudine resistance were 2.6 log copies/ml in HBV DNA (the same as the lower detection limit), 4.0 log U/ml in HBcrAg (solid line) and 3.8 log copies/ml in HBV RNA/DNA (solid line). The upper detection limit of HBV DNA is also shown by a horizontal broken line at 7.6 log copy/ml because 4 patients showed levels higher than the upper detection limit at the baseline.

months after starting lamivudine therapy. The cut-off values of HBV DNA (2.6 log copies/ml), HBcrAg (4.0 log U/ml), and HBV RNA/DNA (3.8 log copies/ml) for prediction of resistance was determined by ROC analysis. The sensitivity, specificity, and accuracy for predicting breakthrough were 25 %, 100 %, and 67 % respectively for HBV DNA. Similarly, they were 100 %, 40 %, and 67 % for HBcrAg, and 50 %, 90 %, and 72 % for HBV RNA/DNA. The positive predictive values for predicting HBV DNA breakthrough by HBV DNA, HBcrAg, and HBV RNA/DNA combined was 100 %, 57.1 %, and 80.0 % respectively. Similarly, the negative predictive values were 63.6 %, 100 %, and 62.5 %.

The cumulative occurrence of HBV DNA breakthrough was compared using a log-rank test between two groups of patients divided by the cut-off values of HBV DNA ($P<0.0003$), HBcrAg ($P=0.0088$), and HBV RNA/DNA ($P=0.0011$) (Fig. 3). All 4 patients whose HBV DNA levels were higher than the cut-off showed lamivudine resistance within 24 months of the start of therapy. None of the 9 patients whose HBcrAg levels were less than the cut-off showed lamivudine resistance during the follow-up period. HBV RNA/DNA showed an intermediate character between HBV DNA and HBcrAg in predicting the occurrence of HBV DNA breakthrough.

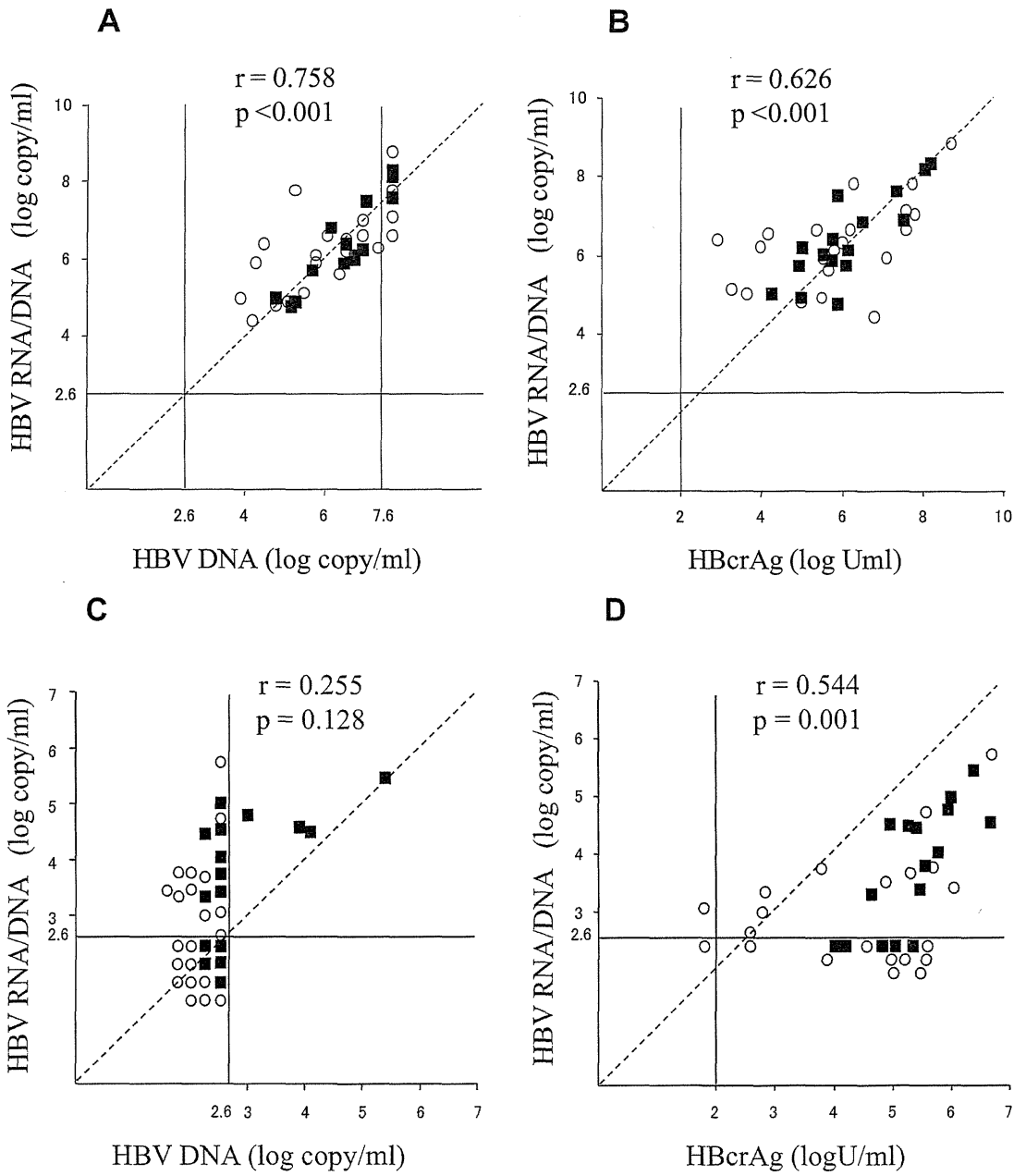

Fig. 2 Correlation between the levels of the three parameters at baseline and at 6 months after starting lamivudine administration: (A) between HBV DNA and HBV RNA/DNA at baseline, (B) between HBcrAg and HBV RNA/DNA at baseline, (C) between HBV DNA and HBV RNA/DNA at 6 months, and (D) between HBcrAg and HBV RNA/DNA at 6 months. Closed squares indicate patients with breakthrough during the observation period, and open circles indicate patients without.

Ⅳ Discussion

HBV is an enveloped DNA virus containing a relaxed circular DNA genome that is converted into a covalently closed circular DNA (cccDNA) episome in the nucleus of infected cells which serves as a transcriptional template for the production of viral RNA. Reverse transcription of pregenomic RNA and second-strand DNA synthesis then occurs in the cytoplasm within viral capsids formed by the HBV core protein. Because lamivudine inhibits reverse transcription of pregenomic RNA, it directly suppresses production of HBV virions, and serum HBV DNA levels decrease rapidly after the initiation of lamivudine administration. On the other hand, the amount of cccDNA decreases quite slowly

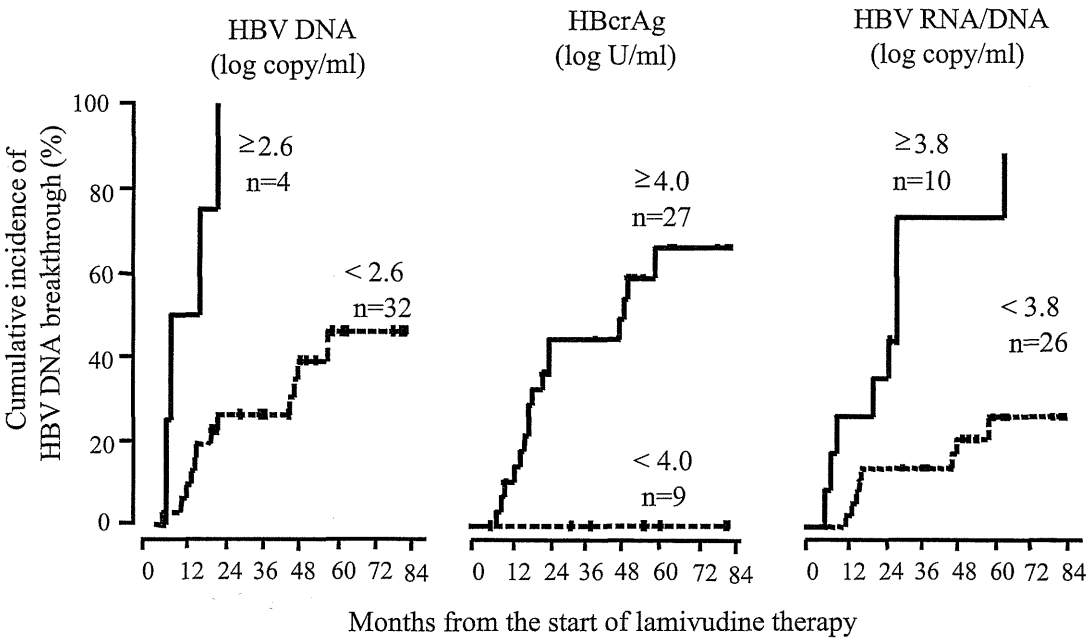

Fig. 3 Cumulative occurrence of HBV DNA breakthrough between two groups of patients classified by the selected cut-off values of HBV DNA (2.6 log copy/ml), HBcrAg (4.0 log U/ml), and HBV RNA/DNA (3.8 copy/ml).

after commencement of nucleoside analogues. Intrahepatic HBV cccDNA has been reported to be superior to serum HBV DNA in predicting virologic response to nucleoside/nucleotide analogue therapies, such as lamivudine[26)–30)]. However, the measurement of cccDNA seems ill-suited for clinical use because it requires a liver biopsy and complicated measurements. The HBcrAg assay developed by our research group has been shown to be useful for identifying patients who are at low risk of developing lamivudine resistance during therapy[21)], as well as those who are at low risk of hepatitis reactivation after cessation of lamivudine administration[31)32)]. The serum HBcrAg levels were well correlated with intrahepatic cccDNA level after HBV DNA became undetectable during anti-viral therapy[33)]. Here, serum HBcrAg may reflect the intrahepatic cccDNA better than serum HBV DNA under lamivudine therapy since lamivudine inhibits the synthesis of HBV DNA from pregenomic RNA transcribed from cccDNA, but does not inhibit synthesis of viral proteins which are translated from viral mRNA directly.

Maturation of the HBV genome occurs in nucleocapsids. Viral polymerase initiates encapsidation by binding to the encapsidation signal, epsilon, and a secondary structure on the pregenomic RNA, which is then complexed with core proteins to form nucleocapsids. The polymerase-epsilon interaction is also the first step in initiating reverse transcription of pregenomic RNA to yield the negative DNA strand of the viral genome[29)32)]. Therefore, we can hypothesize that HBV particles containing pregenomic HBV RNA are produced rather than those containing HBV DNA during lamivudine therapy. Lamivudine inhibits reverse transcription of pregenomic RNA, suggesting that HBV particles containing HBV RNA are produced and may account for the majority of HBV particles[22)]. Accordingly, it is also possible that serum HBV RNA reflects intrahepatic cccDNA and is useful for predicting the occurrence of lamivudine resistance. Recently, Hatakeyama et al. reported that serum HBV RNA was a predictor of early emergence of the YMDD mutant in patients treated with lamivudine[34)]. In a previous study, we demonstrated a method to measure serum HBV RNA only by eliminating HBV DNA. However, this method is prohibitively complicated for testing many samples because it includes a digestion step with DNAase.

As such, HBV DNA and RNA were measured simultaneously in the present study by eliminating the digestion step. Because the proportion of HBV DNA to HBV RNA at 6 months was quite low, we believe that the possibility of HBV RNA as a predictor for lamivudine resistance could be tested.

This study compared the abilities of HBV DNA, HBV RNA/DNA, and HBcrAg for predicting occurrence of lamivudine resistance. Lamivudine resistance was monitored by HBV DNA breakthrough because it is more sensitive than hepatitis breakthrough in detecting resistance. The specificity of HBV DNA breakthrough was confirmed by the existence of YMDD mutations. HBV DNA appears useful for detecting patients who are at high risk of developing lamivudine resistance, but not for selecting patients who are at low risk because the positive predictive value was as high as 100 % and sensitivity as low as 25 %. On the contrary, HBcrAg was useful for identifying patients who are at low risk of lamivudine resistance, but not for patients who are at high risk since the negative predictive value was as high as 100 % and specificity as low as 40 %. HBV DNA breakthrough did not occur until 60 months from the start of lamivudine therapy in 9 patients whose HBcrAg was less than 4.0 log U/ml at 6 months of therapy.

The ability of HBV RNA/DNA for predicting the occurrence of lamivudine resistance landed between those of HBV DNA and HBcrAg ; both the positive (80 %) and negative (63 %) predictive values were intermediate. The accuracy (72 %) of HBV RNA/DNA was highest among the three parameters. Thus, HBV RNA/DNA is presumed to have the predictive characteristics of both HBV DNA and HBcrAg, with the additional feature of including a wider range of patients.

Lamivudine has already been eliminated from first line therapy in naive chronic hepatitis B patients due to a higher incidence of developing resistant mutations than new antiviral agents, such as adefovir dipivoxil and entecavir. However, a considerable number of patients who began lamivudine administration in the past still take this treatment, so the present study may be valuable to such patients when they consider changing therapies in the future. For example, lamivudine patients who show low levels of HBV RNA/DNA or HBcrAg do not necessarily need to change their therapy to a new antiviral regimen. Additionally, since the main mechanisms of suppressing HBV replication are similar among lamivudine, entecavir, and adefovir dipivoxil, it is possible that HBV DNA, HBV RNA/DNA, and HBcrAg are useful for monitoring the antiviral effects of these drugs as well. However, further studies are required to determine whether these three assays are indeed applicable to antiviral agents other than lamivudine.

In conclusion, monitoring HBV DNA is useful for identifying patients with chronic hepatitis B under lamivudine therapy who are at high risk of lamivudine resistance, and measurement of HBcrAg is useful for isolating those who are at low risk of HBV DNA breakthrough. The predictive characteristics of HBV RNA/DNA are similar to that of HBV DNA with higher sensitivity, and show the highest accuracy.

V Acknowledgement

This research was supported in part by a research grant on hepatitis from the Japanese Ministry of Health, Labor and Welfare (no. 19590757).

References

1) Liaw YF, Sung JJ, Chow WC, Farrell G, Lee CZ, Yuen H, Tanwandee T, Tao QM, Shue K, Keene ON, Dixon JS, Gray DF, Sabbat J : Lamivudine for patients with chronic hepatitis B and advanced liver disease. N Engl J Med 351 : 1521-1531, 2004

2) Matsumoto A, Tanaka E, Rokuhara A, Kiyosawa K, Kumada H, Omata M, Okita K, Hayashi N, Okanoue T, Iino S, Tanikawa K : Efficacy of lamivudine for preventing hepatocellular carcinoma in chronic hepatitis B : A multicenter retrospective study of 2,795 patients. Hepatology Research 32 : 173-184, 2005

3) Leung NW, Lai CL, Chang TT, Gran R, Lee CM, Ng KY, Lim SG, Wu PC, Dent JC, Edmundson S, Condreay LD, Chien RN ; Asia Hepatitis Lamivudine Study Group : Extended lamivudine treatment in patients with chronic hepatitis B enhances hepatitis B e antigen seroconversion rates : results after 3 years of therapy. Hepatology 33 : 1527-1532, 2001
4) Liaw YF, Chien RN, Yeh CT, Tsai SL, Chu CM : Acute exacerbation and hepatitis B virus clearance after emergence of YMDD motif mutation during lamivudine therapy. Hepatology 30 : 567-572, 1999
5) Kim JW, Lee HS, Woo GH, Yoon JH, Jang JJ, Chi JG, Kim CY : Fatal sub massive hepatic necrosis associated with tyrosine-methionine-aspartate-aspartate- motif mutation of hepatitis B virus after long-term lamivudine therapy. Clin Infect Dis 33 : 403-405, 2001
6) Villet S, Pichoud C, Villeneuve JP, Trepo C, Zoulim F : Selection of a multiple drug-resistant hepatitis B virus strain in a liver-transplanted patient. Gastroenterology 131 : 1253-1261, 2006
7) Yim HJ, Hussain M, Liu Y, Wong SN, Fung SK, Lok AS : Evolution of multi-drug resistant hepatitis B virus during sequential therapy. Hepatology 44 : 703-712, 2006
8) Lee YS, Suh DJ, Lim YS, Jung SW, Kim KM, Lee HC, Chung YH, Yoo W, Kim SO : Increased risk of adefovir resistance in patients with lamivudine-resistant chronic hepatitis B after 48 weeks of adefovir dipivoxil monotherapy. Hepatology 43 : 1385-1391, 2006
9) Dienstag JL, Goldin RD, Heathcote EJ, Hann HW, Woessner M, Stephenson SL, Gardner S, Gray DF, Schiff ER : Histological outcome during long-term lamivudine therapy. Gastroenterology 124 : 105-117, 2003
10) Dienstag JL, Perrillo RP, Schiff ER, Bartholomew M, Vicary C, Rubin M : A Preliminary trial of lamivudine for chronic hepatitis B infection. N Engl J Med 333 : 1657-1661, 1995
11) Doong SL, Tsai CH, Schinazi RF, Liotta DC, Cheng YC : Inhibition of the replication of hepatitis B virus in vitro by 2',3'-dideoxy-3'-thiacytidine and related analogues. Proc Natl Acad Sci U S A 88 : 8495-8499, 1991
12) Lai CL, Chien RN, Leung NW, Chang TT, Guan R, Tai DI, Ng KY, Wu PC, Dent JC, Barber J, Stephenson SL, Gray DF : A one-year trial of lamivudine for chronic hepatitis B. Asia Hepatitis Lamivudine Study Group. N Engl J Med 339 : 61-68, 1998
13) Liaw YF, Chien RN, Yeh CT, Tsai SL, Chu CM : Acute exacerbation and hepatitis B virus clearance after emergence of YMDD motif mutation during lamivudine therapy. Hepatology 30 : 567-572, 1999
14) Nafa S, Ahmed S, Tavan D, Pichoud C, Berby F, Stuyver L, Johnson M, Merle P, Abidi H, Trepo C, Zoulim F : Early detection of viral resistance by determination of hepatitis B virus polymerase mutations in patients treated by lamivudine for chronic hepatitis B. Hepatology 32 : 1078-1088, 2000
15) Yuen MF, Kato T, Mizokami M, Chan AO, Yuen JC, Yuan HJ, Wong DK, Sum SM, Ng IO, Fan ST, Lai CL : Clinical outcome and virologic profiles of severe hepatitis B exacerbation due to YMDD mutations. J Hepatol 39 : 850-855, 2003
16) Kumashiro R, Kuwahara R, Ide T, Koga Y, Arinaga T, Hisamochi A, Ogata K, Tanaka K, Sata M : Subclones of drug-resistant hepatitis B virus mutants and the outcome of breakthrough hepatitis in patients treated with lamivudine. Intervirology 46 : 350-354, 2003
17) Suzuki F, Tsubota A, Arase Y, Suzuki Y, Akuta N, Hosaka T, Someya T, Kobayashi M, Saitoh S, Ikeda K, Kobayashi M, Matsuda M, Satoh J, Takagi K, Kumada H : Efficacy of lamivudine therapy and factors associated with emergence of resistance in chronic hepatitis B virus infection in Japan. Intervirology 46 : 182-189, 2003
18) Zollner B, Schafer P, Feucht HH, Schroter M, Petersen J, Laufs R : Correlation of hepatitis B virus load with loss of e antigen and emerging drug-resistant variants during lamivudine therapy. J Med Virol 65 : 659-663, 2001
19) Rokuhara A, Tanaka E, Matsumoto A, Kimura T, Yamaura T, Orii K, Sun X, Yagi S, Maki N, Kiyosawa K : Clinical evaluation of a new enzyme immunoassay for hepatitis B virus core-related antigen ; a marker distinct from viral DNA for monitoring lamivudine treatment. J Viral Hepat 10 : 324-330, 2003
20) Kimura T, Ohno N, Terada N, Rokuhara A, Matsumoto A, Yagi S, Tanaka E, Kiyosawa K, Ohno S, Maki N : Hepatitis B virus DNA-negative dane particles lack core protein but contain a 22-kDa precore protein without C-terminal arginine-rich domain. J Biol Chem 280 : 21713-21719, 2005
21) Tanaka E, Matsumoto A, Suzuki F, Kobayashi M, Mizokami M, Tanaka Y, Okanoue T, Minami M, Chayama K,

Imamura M, Yatsuhashi H, Nagaoka S, Yotsuyanagi H, Kawata S, Kimura T, Maki N, Iino S, Kiyosawa K : Measurement of hepatitis B virus core-related antigen is valuable for identifying patients who are at low risk of lamivudine resistance. Liver Int 26 : 90-96, 2006

22) Rokuhara A, Matsumoto A, Tanaka E, Umemura T, Yoshizawa K, Kimura T, Maki N, Kiyosawa K : Hepatitis B Virus RNA is Measurable in Serum and can be a New Marker for Monitoring Lamivudine Therapy. J Gastroenterol 41 : 785-790, 2006

23) Mizokami M, Nakano T, Orito E, Tanaka Y, Sakugawa H, Mukaide M, Robertson BH : Hepatitis B virus genotype assignment using restriction fragment length polymorphism patterns. FEBS Lett 450 : 66-71, 1999

24) Kobayashi S, Shimada K, Suzuki H, Tanikawa K, Sata M : Development of a new method for detecting a mutation in the gene encoding hepatitis B virus reverse transcriptase active site (YMDD motif). Hepatol Res 17 : 31-42, 2000

25) Kimura T, Rokuhara A, SakamotoY, Yagi S, Tanaka E, Kiyosawa K, Maki N : Sensitive enzyme immunoassay for hepatitis B virus core-related antigens and their correlation to virus load. J Clin Microbiol 40 : 439-445, 2002

26) Lee WM : Hepatitis B virus infection. N Engl J Med 337 : 1733-1745, 1997

27) Mason WS, Halpern MS, England JM, Seal G, Egan J, Coates L, Aldrich C, Summers J : Experimental transmission of duck hepatitis B virus. Virology 131 : 375-384, 1983

28) Summers J, Mason WS : Replication of the genome of a hepatitis B--like virus by reverse transcription of an RNA intermediate. Cell 29 : 403-415, 1982

29) Tuttleman JS, Pourcel C, Summers J : Formation of the pool of covalently closed circular viral DNA in hepadnavirus-infected cells. Cell 47 : 451-460, 1986

30) Sung JJ, Wong ML, Bowden S, Liew CT, Hui AY, Wong VW, Leung NW, Locarnini S, Chan HL : Intrahepatic hepatitis B virus covalently closed circular DNA can be a predictor of sustained response to therapy. Gastroenterology 128 : 1890-1897, 2005

31) Shinkai N, Tanaka Y, Orito E, Ito K, Ohno T, Hirashima N, Hasegawa I, Sugauchi F, Ueda R, Mizokami M : Measurement of hepatitis B virus core-related antigen as predicting factor for relapse after cessation of lamivudine therapy for chronic hepatitis B virus infection. Hepatol Res 36 : 272-276, 2006

32) Matsumoto A, Tanaka E, Minami M, Okanoue T, Yatsuhashi H, Nagaoka S, Suzuki F, Kobayashi M, Chayama K, Imamura M, Yotsuyanagi H, Nakaoka S, Maki N, Kawata S, Kumada H, Iino S, Kiyosawa K : Low serum level of hepatitis B virus core-related antigen indicates unlikely reactivation of hepatitis after cessation of lamivudine therapy. Hepatol Res 37 : 661-666, 2007

33) Suzuki F, Miyakoshi H, Kobayashi M, Kumada H : Correlation between serum hepatitis B virus core-related antigen and intrahepatic covalently closed circular DNA in chronic hepatitis B patients. J Med Virol 81 : 27-33, 2009

34) Hatakeyama T, Noguchi C, Hiraga N, Mori N, Tsuge M, Imamura M, Takahashi S, Kawakami Y, Fujimoto Y, Ochi H, Abe H, Maekawa T, Kawakami H, Yatsuji H, Aisaka Y, Kohno H, Aimitsu S, Chayama K : Serum HBV RNA is a predictor of early emergence of the YMDD mutant in patients treated with lamivudine. Hepatology 45 : 1179-1186, 2007

(2010. 3. 17 received ; 2010. 5. 7 accepted)

GASTROENTEROLOGY 2010;139:1190–1197

ITPA Polymorphism Affects Ribavirin-Induced Anemia and Outcomes of Therapy—A Genome-Wide Study of Japanese HCV Virus Patients

HIDENORI OCHI,[*,‡] TOSHIRO MAEKAWA,[*] HIROMI ABE,[‡] YASUFUMI HAYASHIDA,[‡] RIKITA NAKANO,[§] MICHAKI KUBO,[‖] TATSUHIKO TSUNODA,[¶] C. NELSON HAYES,[*,‡] HIROMITSU KUMADA,[#] YUSUKE NAKAMURA,[**] and KAZUAKI CHAYAMA[*,‡]

*Laboratory for Liver Diseases, RIKEN Center for Genomic Medicine, Hiroshima, Japan; ‡Department of Medical and Molecular Science, Division of Frontier Medical Science, Programs for Biomedical Research, Graduate School of Biomedical Science, Hiroshima University, Hiroshima, Japan; §Pharmacology Research Laboratories, Drug Research Division, Dainippon Sumitomo Pharma Co, Ltd, Osaka, Japan; ‖Laboratory for Genotyping Development, RIKEN Center for Genomic Medicine, Kanagawa, Japan; ¶Laboratory for Medical Informatics, RIKEN Center for Genomic Medicine, Kanagawa, Japan; #Department of Hepatology, Toranomon Hospital, Tokyo, Japan; and **Laboratory of Molecular Medicine, Human Genome Center, The Institute of Medical Science, University of Tokyo, Tokyo, Japan*

BACKGROUND & AIMS: Ribavirin-induced anemia is one of the major causes of discontinuation and dose reduction during anti-hepatitis C virus therapy. Factors influencing this anemia, especially host genetic factors, are poorly understood. In this study we investigated predictive factors in hepatitis C virus patients treated with combination therapy. **METHODS:** We performed a 2-step genome-wide screening followed by replication analysis and fine-mapping using a total of 923 Japanese hepatitis C virus 1b–infected patients treated with pegylated-interferon plus ribavirin. We also applied logistic regression analysis to search for possible independent associations of clinical parameters and genetic variants with treatment-induced hemoglobin (Hb) decline as well as treatment outcomes. **RESULTS:** We identified a variant, located upstream of the inosine triphosphate pyrophosphatase gene on chromosome 20p13 that is significantly associated with treatment-induced anemia (combined $P = 6.0 \times 10^{-14}$). Resequencing and fine-mapping revealed several single nucleotide polymorphisms (SNPs) strongly associated with Hb decline, including the nonsynonymous SNP rs1127354 ($P = 3.5 \times 10^{-44}$), which was recently reported for other ethnic groups. Another reported SNP, the splicing variant-related SNP rs7270101, was not polymorphic in the Japanese population. Stratified analysis based on rs1127354 genotype revealed that inosine triphosphate pyrophosphatase expression is not correlated with Hb decline, suggesting that rs1127354 is a direct causal variant in the Japanese population. Multivariate analysis demonstrated that age, baseline Hb, baseline platelet count, and rs1127354 were independently associated with severe anemia (Hb <10 g/dL). **CONCLUSIONS: A missense substitution in inosine triphosphate pyrophosphatase gene affects ribavirin-induced anemia in hepatitis C virus–infected Japanese patients.**

Keywords: Hemolysis; Side Effect; SNP.

Hepatitis C virus (HCV) is one of the major causes of liver cirrhosis and hepatocellular carcinoma.[1] Sustained viral response, defined as negative for HCV RNA for 24 weeks after cessation of therapy, can be achieved by the current treatment regimen of pegylated-interferon (PEG-IFN) combined with ribavirin, but this outcome can be attained in <50% of patients infected with genotype 1 HCV.[2,3] Hemolysis is a common side effect of ribavirin and is the major reason for dose reduction. Age,[4,5] female sex,[4] baseline platelet level,[6] baseline hemoglobin (Hb) level,[5] dose,[4] plasma concentration[7] of ribavirin, and haptoglobin phenotype[6] have been reported to contribute to ribavirin-induced anemia and dose reduction. The extent of anemia caused by ribavirin varies greatly among individuals, suggesting a genetic influence. Recently, using a genome-wide association technique, Fellay et al reported that functional variants in inosine triphosphate pyrophosphatase (ITPA), including one coding and one intronic variant, were associated with treatment-induced anemia in HCV-infected patients.[8]

In this report, we describe the results of a genome-wide scan and fine-mapping of anemia in Japanese HCV patients treated with PEG-IFN and ribavirin combination therapy. We replicated the finding of Fellay et al that a nonsynonymous SNP in the ITPA gene is correlated with incidence of anemia. Moreover, we provide evidence suggesting that this variant is also associated with the outcomes of treatment with PEG-IFN and ribavirin combined therapy.

Abbreviations used in this paper: GWAS, genome-wide association study; Hb, hemoglobin; HCV, hepatitis C virus; ITPA, inosine triphosphate pyrophosphatase; LD, linkage disequilibrium; PCR, polymerase chain reaction; PEG-IFN, pegylated-interferon; SNP, single nucleotide polymorphism.

0016-5085/$36.00
doi:10.1053/j.gastro.2010.06.071

Table 1. Clinical Characteristics of the Patients

	GWAS-1	GWAS-2	Replication-1
n	453	212	258
Age, *y*, mean (SD)	57.4 (11.2)	58.7 (10.8)	55.3 (12.7)
Sex, M/F, n	269/184	108/104	134/124
Weight, *kg*, mean (SD)	60.2 (10.3)	59.4 (10.4)	60.8 (11.8)
Body mass index,[a] mean (SD)	23 (2.9)	23.1 (2.9)	23.2 (3.3)
Baseline platelet count, $\times 1000/mm^3$, mean (SD)	158 (52)	154 (57)	165 (60)
Baseline hemoglobin level, *g/dL*, mean (SD)	14 (1.4)	13.9 (1.5)	13.9 (1.6)
Initial ribavirin dose, *mg/d*, n (%)			
200	30 (6.6)	3 (1.4)	19 (7.4)
400	42 (9.3)	28 (13.2)	38 (14.7)
600	200 (44.2)	89 (42)	118 (45.7)
800	170 (37.5)	84 (39.6)	76 (29.5)
1000	11 (2.4)	8 (3.8)	7 (2.7)
Hemoglobin level at week 4, mean (SD)	12 (1.7)	11.9 (1.6)	12.0 (1.7)
Hemoglobin decline at week 4, mean (SD)	2 (1.5)	2.0 (1.6)	1.9 (1.6)
Severe anemia at week 4, n (%)	42 (9.3)	17 (8.0)	32 (12.4)
Fibrosis, mild (F0-F2)/severe (F3-F4), n (%)	175/219 (44.0)	78/92 (45.9)	94/123 (43.3)
HCV genotype	1b	1b	1b

GWAS, genome-wide association study; HCV, hepatitis C virus; M/F, male/female; SD, standard deviation.
[a]Calculated as kg/m^2.

Patients and Methods

Study Population

In this study, we adopted a 2-step genome-wide association study (GWAS) consisting of a screening phase (GWAS-1 and -2) and a subsequent replication analysis (Replication-1) using a total of 923 subjects. Samples of the GWAS-1 were genotyped in the context of another genome-wide study concerning the genetics of treatment response to HCV therapy. The demographic features of the subjects are shown in Table 1. All patients were infected with HCV genotype 1b and treated with PEG-IFN plus ribavirin between 2003 and 2008 at either Toranomon Hospital Department of Hepatology or at Hiroshima University-affiliated hospitals. All patients had abnormal levels of serum alanine transaminase for more than 6 months and were positive for both anti-HCV antibody and serum HCV RNA. All patients were negative for hepatitis B surface antigen, had no evidence of other liver diseases, and had not received immunosuppressive therapy before enrollment in the study. Patients received weekly injections of PEG-IFN-α-2b at 1.5 μg/kg body weight and oral administration of ribavirin for 48 weeks. The amount of ribavirin was adjusted based on the subject's body weight (600 mg for <60 kg, 800 mg for 60−80 kg, 1000 mg for >80 kg). Patients with hemoglobin concentrations of <12 g/dL were given reduced dose of ribavirin (200 mg lower than standard dose determined by body weight) to prevent early discontinuation of the therapy. All subjects in the present study gave written informed consent to participate in the study according to the process approved by the Ethical Committee at the SNP Research Center, the Institute of Physical and Chemical Research (RIKEN), Yokohama, and conforming to the ethical guidelines of the 1975 Declaration of Helsinki.

Genotyping and Quality Control

To identify causal variants for ribavirin-induced anemia, we applied a 2-stage approach for GWAS screening. In GWAS-1 we analyzed 453 samples using the Illumina HumanHap 610-Quad Genotyping BeadChip (San Diego, CA). Genotyping data were subjected to quality control before analysis. Genotyping for GWAS-2 and Replication-1 was performed using the Invader assay (Third Wave Technologies, Madison, WI), the TaqMan assay (Applied Biosystems, Foster City, CA), or by direct sequencing as described previously.[9,10]

Fine-Mapping Analysis

After the association analysis, fine-mapping was performed on the region surrounding the top marker. Using Phase II HapMap JPT genotype data, linkage disequilibrium (LD) blocks were defined by the Haploview program (http://www.broadinstitute.org/mpg/haploview/).[11] Resequencing around the top marker was also performed by direct sequencing of DNA from 48 unrelated Japanese HCV patients from the enrolled subjects. Using the Haploview program, tag SNPs were selected from among the identified SNPs based on a selection criteria of r^2 >0.8, and the tag SNPs were genotyped for all enrolled patients.

HCV RNA Level

The HCV RNA level was analyzed before interferon therapy, using reverse transcription polymerase chain reaction (PCR)−based methods (the high range method or the TaqMan reverse transcription-PCR test).